The Astrophysical Journal, 747:73 (12pp), 2012 March 1 doi:10.1088/0004-637X/747/1/73

ON THE REQUIREMENTS FOR REALISTIC MODELING OF NEUTRINO TRANSPORT IN SIMULATIONS OF CORE-COLLAPSE SUPERNOVAE

Eric J. Lentz[1,2,3], Anthony Mezzacappa[2,4,8], O. E. Bronson Messer[4,5,8], Matthias Liebendörfer[6], W. Raphael Hix[2,8], and Stephen W. Bruenn[7]
[1] Department of Physics and Astronomy, University of Tennessee, Knoxville, TN 37996-1200, USA; elentz@utk.edu
[2] Physics Division, Oak Ridge National Laboratory, P.O. Box 2008, Oak Ridge, TN 37831-6354, USA; mezzacappaa@ornl.gov
[3] Joint Institute for Heavy Ion Research, Oak Ridge National Laboratory, P.O. Box 2008, Oak Ridge, TN 37831-6374, USA
[4] Computer Science and Mathematics Division, Oak Ridge National Laboratory, P.O. Box 2008, Oak Ridge, TN 37831-6164, USA
[5] National Center for Computational Sciences, Oak Ridge National Laboratory, P.O. Box 2008, Oak Ridge, TN 37831-6164, USA
[6] Department of Physics, University of Basel, Klingelbergstrasse 82, CH-4056 Basel, Switzerland
[7] Department of Physics, Florida Atlantic University, 777 Glades Road, Boca Raton, FL 33431-0991, USA
Received 2011 October 12; accepted 2011 December 15; published 2012 February 15

ABSTRACT

We have conducted a series of numerical experiments with the spherically symmetric, general relativistic, neutrino radiation hydrodynamics code AGILE-BOLTZTRAN to examine the effects of several approximations used in multidimensional core-collapse supernova simulations. Our code permits us to examine the effects of these approximations quantitatively by removing, or substituting for, the pieces of supernova physics of interest. These approximations include: (1) using Newtonian versus general relativistic gravity, hydrodynamics, and transport; (2) using a reduced set of weak interactions, including the omission of non-isoenergetic neutrino scattering, versus the current state-of-the-art; and (3) omitting the velocity-dependent terms, or observer corrections, from the neutrino Boltzmann kinetic equation. We demonstrate that each of these changes has noticeable effects on the outcomes of our simulations. Of these, we find that the omission of observer corrections is particularly detrimental to the potential for neutrino-driven explosions and exhibits a failure to conserve lepton number. Finally, we discuss the impact of these results on our understanding of current, and the requirements for future, multidimensional models.

Key words: methods: numerical – neutrinos – radiative transfer – supernovae: general

Online-only material: color figures

1. INTRODUCTION

Colgate and White (1966) were the first to propose that core-collapse supernovae may be neutrino-driven and performed the first numerical simulations of such events, launching more than four decades of research that continues to this day. A significant milestone occurred nearly two decades later with Wilson's discovery that delayed neutrino-driven explosions could be obtained. Based on his models, Wilson concluded (Wilson 1985; Bethe & Wilson 1985) that the stalled supernova shock wave could be revived via neutrino absorption on a time scale of several hundred milliseconds given the intense flux of neutrinos emerging from the proto-neutron star (proto-NS) liberating the star's gravitational binding energy. Observations of the neutrinos from SN1987A, the first such observations of supernova neutrinos (Bionta et al. 1987; Hirata et al. 1987), provided support for the central role of neutrinos in the explosion mechanism. State-of-the-art simulations today continue to explore Wilson's neutrino-driven explosion mechanism in the context of two-dimensional (2D) and three-dimensional (3D) models (e.g., see Burrows et al. 2007; Marek & Janka 2009; Bruenn et al. 2009; Suwa et al. 2010).

Neutrinos are weakly interacting particles whose cross sections are energy dependent. Thus, unlike all other components in a supernova model, they are not well described as a fluid, except in the deepest layers, and their transition in space to non-fluid-like behavior depends on their energy. Instead, the evolution of the neutrino radiation field, particularly in the semi-transparent regime, is far better characterized by classical kinetics—specifically, the general relativistic Boltzmann kinetic equation (e.g., see Cardall & Mezzacappa 2003),

$$p^{\hat{\mu}}\left(\Lambda^{\bar{\mu}}{}_{\hat{\mu}}e^{\mu}{}_{\bar{\mu}}\frac{\partial f}{\partial x^{\mu}}-\Gamma^{\hat{\nu}}{}_{\hat{\rho}\hat{\mu}}p^{\hat{\rho}}\frac{\partial f}{\partial p^{\hat{\nu}}}\right)=C[f], \tag{1}$$

where, for spherical symmetry,

$$\begin{aligned}\frac{1}{E}C[f]=&(1-f)j-\chi f\\&+\frac{1}{c}\frac{1}{h^3c^3}E^2\int d\mu' R_{\rm IS}(\mu,\mu',E)f\\&-\frac{1}{c}\frac{1}{h^3c^3}E^2 f\int d\mu' R_{\rm IS}(\mu,\mu',E)\\&+\frac{1}{h^3c^4}(1-f)\int dE'E'^2 d\mu' R^{\rm in}_{\rm NIS}(\mu,\mu',E,E')f\\&-\frac{1}{h^3c^4}f\int dE'E'^2 d\mu' R^{\rm out}_{\rm NIS}(\mu,\mu',E,E')(1-f)\\&+\frac{1}{h^3c^4}(1-f)\int dE'E'^2 d\mu'\\&\quad\times R^{\rm in}_{\rm PR}(\mu,\mu',E,E')(1-\bar{f})\\&-\frac{1}{h^3c^4}f\int dE'E'^2 d\mu' R^{\rm out}_{\rm PR}(\mu,\mu',E,E')\bar{f}.\end{aligned} \tag{2}$$

Equation (1) describes the evolution of the neutrino distribution function $f(t, x_1, x_2, x_3, \mu_1, \mu_2, E)$, which at time t and spatial location (x_1, x_2, x_3) supplies the distribution of neutrinos in direction cosines (μ_1, μ_2) and energy E—i.e., the angular and spectral distribution of neutrinos. One such Boltzmann equation

[8] Also at the Department of Physics and Astronomy, University of Tennessee.

is solved for each flavor of neutrino—electron, muon, and tau (ν_e, ν_μ, and ν_τ, respectively)—and for their antineutrino partners ($\bar{\nu}_e$, $\bar{\nu}_\mu$, and $\bar{\nu}_\tau$). The invariant collision term, $C[f]$, in Equation (2) is written using emission j, absorption χ, and scattering and pair kernels R, following the forms often used for neutrino transport (e.g., see Mezzacappa & Messer 1999), where $\bar{f}$ is the distribution function for the partner antineutrino and μ is the neutrino direction cosine. In Equations (1) and (2), f is a function of (μ, E), as well as position and time. The (μ', E') dependence of f and $\bar{f}$ inside the integrals illustrates the physical coupling of all energies and angles for each neutrino species and of neutrino and antineutrino partners.

The first term on the left-hand side of Equation (1) describes the time evolution of the local neutrino distribution owing to spatial transport through the volume of interest. The second, far more complex term on the left-hand side (LHS/Term 2) describes the evolution of the local neutrino distribution in angle and energy as the result of (A) the coordinate system chosen, (B) special relativistic effects, and (C) general relativistic effects. In what follows, we will refer to (B) as "observer corrections."

Terms describing (A) depend on the choice of coordinate system. For example, in spherical polar coordinates, the neutrino direction cosine relative to the outwardly pointing radial vector changes as the neutrino propagates through a local volume. This coordinate-system effect is included in LHS/Term 2 and is present even in the absence of fluid motion or general relativity. For Cartesian coordinates, the neutrino direction cosines do not change as a result of the coordinate system choice alone and, consequently, such a term is absent.

Terms describing (B) depend on the frame of reference chosen to measure the neutrino direction cosines and energies. The comoving frame, with neutrino direction cosines and energies measured in an inertial frame of reference instantaneously comoving with the stellar core fluid with which the neutrinos interact, is often used. Neutrino–matter interactions are naturally expressed in this frame. Given this choice, the terms in LHS/Term 2 present a significant numerical challenge. Finding discrete representations that guarantee conservation of lepton number and energy is one of the most difficult aspects of modeling neutrino transport in stellar cores. This has been achieved for general relativistic, spherically symmetric flows (Liebendörfer et al. 2004), providing the conceptual and implementation groundwork for achieving the same in axisymmetric (2D) and non-symmetric (3D) flows. Further theoretical foundations have been laid (Cardall & Mezzacappa 2003; Cardall et al. 2005); steps toward the development of a 2D Boltzmann solver have been taken (Ott et al. 2008); and the challenge now is to fully implement lepton energy and number conserving discretizations in 2D and 3D models.

For another choice of reference frame—measuring neutrino angles and energies relative to the inertial, "lab" frame of a distant observer—the terms encapsulating the special relativistic effects in LHS/Term 2 are absent, simplifying the left-hand side of the Boltzmann equation. In such a frame of reference, the neutrino direction cosines and energies do not change from observer to observer in the frame. However, this simplification comes at a price because the neutrino–matter interactions are naturally described in the comoving frame. In the lab frame, a Lorentz transformation is required in order to express the comoving-frame neutrino–matter interactions in terms of the lab-frame direction cosines and energies, which introduces nontrivial velocity dependencies into the lab-frame collision term.

One approach to the complexity of the lab-frame collision term is the "mixed frame" approach, which uses the lab-frame four-momenta and an $\mathcal{O}(v/c)$ Taylor-series expansion in energy of the comoving-frame emissivities and opacities (Mihalas & Klein 1982). Hubeny & Burrows (2007) have proposed to use the mixed-frame approach for core-collapse simulations with extensions for non-isotropic and non-isoenergetic scattering. The mixed-frame approach may be difficult to extend to arbitrarily relativistic flows, and has not yet been used in the context of a full-physics core-collapse supernova simulation.

In a general relativistic setting, such as core-collapse supernovae, we must contend with (B) and/or (C) regardless of the frame of reference chosen to describe the neutrino direction cosines and energies. Even for static general relativistic environments, angular aberration, gravitational red shift, and other effects occur, and the resulting terms in (C) are always present.

Regardless of approach, comoving- or lab-frame, it is problematic to adapt the simplicity of both approaches, simultaneously simplifying the left- and right-hand sides of the Boltzmann equation, as has been done in Burrows et al. (2006, 2007), Ott et al. (2008), and other models using the Vulcan/2D code, although one can view the implementation in these works as steps toward a more complete description. They deploy a lab-frame approach for terms describing angular aberration and energy shift on the left-hand side (or assume that such terms are unimportant in a comoving-frame approach), while simultaneously deploying a comoving-frame approach for the collision term describing the neutrino–matter interactions on the right-hand side. This is not a mixed-frame approach in the sense described above. It is an approach not based in any reference frame, and it is physical only for static cases in which there is no distinction between lab and comoving frames. One of the goals of this study is to investigate the importance of the terms in LHS/Term 2 in a comoving-frame approach, and whether they can be ignored while using a comoving-frame approach for the collision term.

Modeling general relativistic Boltzmann kinetics is also challenging because of the complexity of the collision term on the right-hand side of the Boltzmann equation, even in a comoving-frame formulation. Looking at Equation (2), we see that the collision term describes the full, direct coupling of all neutrino angles and energies for each neutrino species, owing to neutrino isoenergetic scattering (IS) on nuclei and non-isoenergetic scattering (NIS) on electrons and nucleons. The pair creation and annihilation processes (PR) such as electron–positron annihilation and nucleon–nucleon bremsstrahlung also couple the angles and energies of the neutrino and antineutrino species of each flavor together. The coupling of all neutrino angles and energies through the relevant set of weak interactions dominates the computation associated with the solution of the neutrino Boltzmann equations. It has been argued (Burrows et al. 2006, 2007; Nordhaus et al. 2010) that these couplings are subdominant and can be ignored, greatly simplifying the neutrino Boltzmann equations and significantly reducing the computational cost associated with their solution. A second goal of this study is to investigate whether or not such approximations to the collision term are realistic.

The complete general relativistic Boltzmann equation was solved in spherically symmetric models of core-collapse supernovae by the Oak Ridge–Basel collaboration (Liebendörfer et al. 2001, 2004) and by Sumiyoshi and collaborators (Sumiyoshi et al. 2005). Achieving this in 3D models of core-collapse supernovae presents a major challenge, one that will likely require sustained exascale resources to meet.

The overarching goal of this study is to use general relativistic, spherically symmetric Boltzmann simulations to

guide and, more importantly, set minimum requirements for accurate 2D and 3D simulations. We use the Oak Ridge–Basel code AGILE-BOLTZTRAN in these studies to compare general relativistic–full weak interaction physics (GR-FullOp), Newtonian–full weak interaction physics (N-FullOp), Newtonian–reduced weak interaction physics (N-ReducOp), and Newtonian–reduced weak interaction physics–no observer correction (N-ReducOp-NOC) models. These models will demonstrate the importance of general relativity, a complete weak interaction set and treatment, and the terms in LHS/Term 2 to stellar core collapse and the post-core-bounce evolution. Current multidimensional models suggest that spherical symmetry is a reasonable approximation for the first 100–150 ms after bounce (Marek & Janka 2009; Bruenn et al. 2009; Suwa et al. 2010). Thus, the simulations presented here are relevant for discussing the initial conditions present for all multidimensional phenomena that might ensue; e.g., neutrino-driven convection and the standing accretion shock instability (SASI).

2. DISABLING OBSERVER CORRECTIONS IN A LAGRANGIAN FORMULATION

Disabling general relativity in a simulation, instead running a Newtonian simulation, is straightforward and requires no special considerations to define or interpret. The same holds true for limiting the weak interaction channels included in the collision term on the right-hand side of the Boltzmann equation. Newtonian or general relativistic simulations can be performed with more, or less, weak interaction physics. However, disabling the observer corrections in a model requires some definition and care.

Using Mezzacappa & Matzner (1989), Equation (VI.11), we begin by expressing the neutrino Boltzmann equation in flat spacetime, Eulerian spherical polar spacetime coordinates with zero shift vector, comoving-frame four-momenta, and in nonconservative form:

$$\begin{aligned}&\frac{\partial f}{\partial \tilde{t}}+\frac{\mu_0+v}{1+\mu_0 v}\frac{\partial f}{\partial r}\\&\quad+\left[\frac{1}{r}-\gamma^2\left(\frac{\partial v}{\partial \tilde{t}}+\frac{\mu_0+v}{1+\mu_0 v}\frac{\partial v}{\partial r}\right)\right]\left(1-{\mu_0}^2\right)\frac{\partial f}{\partial \mu_0}\\&\quad-\left[\frac{1-{\mu_0}^2}{1+\mu_0 v}\frac{v}{r}+\mu_0\gamma^2\left(\frac{\partial v}{\partial \tilde{t}}+\frac{\mu_0+v}{1+\mu_0 v}\frac{\partial v}{\partial r}\right)\right]E_0\frac{\partial f}{\partial E_0}\\&=\frac{1}{\gamma E_0}\frac{1}{1+\mu_0 v}(e-of)\\&\equiv\frac{1}{\gamma E_0}\frac{1}{1+\mu_0 v}C[f].\end{aligned}$$

In Equation (3), μ_0 and E_0 are the neutrino direction cosine and energy as measured in a comoving frame of reference, and e and o are the invariant emissivity and opacity. We use $c = 1$ throughout this section, and have written the Eulerian time coordinate as $\tilde{t}$. Multiplying by $(1+\mu_0 v)$ and rearranging we have

$$\begin{aligned}&(1+\mu_0 v)\frac{\partial f}{\partial \tilde{t}}+(\mu_0+v)\frac{\partial f}{\partial r}+\frac{1-{\mu_0}^2}{r}\frac{\partial f}{\partial \mu_0}\\&\quad+\left[\left(\frac{v}{r}-\frac{\partial v}{\partial r}\right)\mu_0\left(1-{\mu_0}^2\right)+\mathcal{O}(v^2)\right]\frac{\partial f}{\partial \mu_0}\\&\quad+\left[{\mu_0}^2\left(\frac{v}{r}-\frac{\partial v}{\partial r}\right)-\frac{v}{r}+\mathcal{O}(v^2)\right]E_0\frac{\partial f}{\partial E_0}=\frac{1}{E_0}C[f].\end{aligned}\tag{4}$$

Using the continuity equation,

$$\frac{1}{\rho}\frac{D\rho}{D\tilde{t}}+\frac{3v}{r}=\frac{v}{r}-\frac{\partial v}{\partial r},$$

where $D/D\tilde{t}=\partial/\partial\tilde{t}+v\partial/\partial r$, Equation (4), and dropping $\mathcal{O}(v^2)$ terms we get

$$\begin{aligned}&(1+\mu_0 v)\frac{\partial f}{\partial \tilde{t}}+(\mu_0+v)\frac{\partial f}{\partial r}+\frac{1-{\mu_0}^2}{r}\frac{\partial f}{\partial \mu_0}\\&\quad+\left(\frac{1}{\rho}\frac{D\rho}{D\tilde{t}}+\frac{3v}{r}\right)\mu_0\left(1-{\mu_0}^2\right)\frac{\partial f}{\partial \mu_0}\\&\quad+\left[{\mu_0}^2\left(\frac{1}{\rho}\frac{D\rho}{D\tilde{t}}+\frac{3v}{r}\right)-\frac{v}{r}\right]E_0\frac{\partial f}{\partial E_0}=\frac{1}{E_0}C[f].\end{aligned}\tag{5}$$

We can express the observer correction terms in conservative form using

$$\mu_0\left(1-{\mu_0}^2\right)\frac{\partial f}{\partial \mu_0}=\frac{\partial\left[\mu_0\left(1-{\mu_0}^2\right)f\right]}{\partial \mu_0}-f\left(1-3{\mu_0}^2\right)$$

and

$$E_0\frac{\partial f}{\partial E_0}=\frac{1}{{E_0}^2}\frac{\partial\left({E_0}^3 f\right)}{\partial E_0}-3f.$$

Substituting these expressions into Equation (5), we get the $\mathcal{O}(v)$ Boltzmann equation,

$$\begin{aligned}&(1+\mu_0 v)\frac{\partial f}{\partial \tilde{t}}+(\mu_0+v)\frac{\partial f}{\partial r}+\frac{1-{\mu_0}^2}{r}\frac{\partial f}{\partial \mu_0}\\&\quad+\left(\frac{1}{\rho}\frac{D\rho}{D\tilde{t}}+\frac{3v}{r}\right)\frac{\partial\left[\mu_0\left(1-{\mu_0}^2\right)f\right]}{\partial \mu_0}\\&\quad+\left[{\mu_0}^2\left(\frac{1}{\rho}\frac{D\rho}{D\tilde{t}}+\frac{3v}{r}\right)-\frac{v}{r}\right]\frac{1}{{E_0}^2}\frac{\partial\left({E_0}^3 f\right)}{\partial E_0}-\frac{1}{\rho}\frac{D\rho}{D\tilde{t}}f\\&\quad=\frac{1}{E_0}C[f].\end{aligned}\tag{6}$$

Note that the last term on the left-hand side of Equation (6), $-(f/\rho)D\rho/D\tilde{t}$, is part of the observer corrections.

Our Eulerian starting point with comoving-frame neutrino four-momenta (Equation (4)) provides the formulation in which we can most readily discuss what it means to have Boltzmann neutrino transport without observer corrections. We define the evolution of the neutrino distributions in this case to be governed by

$$(1+\mu_0 v)\frac{\partial f}{\partial \tilde{t}}+(\mu_0+v)\frac{\partial f}{\partial r}+\frac{1-{\mu_0}^2}{r}\frac{\partial f}{\partial \mu_0}=\frac{1}{E_0}C[f];\tag{7}$$

that is, by Equation (4) with the velocity-dependent, neutrino angle- and energy-shift terms ignored.

From Equations (15)–(22) of Liebendörfer et al. (2004), AGILE-BOLTZTRAN evolves the following purely Lagrangian (comoving-frame spacetime coordinates and neutrino four-momenta) equations in flat spacetime,

$$\begin{aligned}&\frac{\partial F}{\partial t}+4\pi\mu_0\frac{\partial\left(r^2\rho F\right)}{\partial m}+\frac{1}{r}\frac{\partial\left[\left(1-{\mu_0}^2\right)F\right]}{\partial \mu_0}+\left(\frac{1}{\rho}\frac{\partial\rho}{\partial t}+\frac{3v}{r}\right)\\&\quad\times\frac{\partial\left[\mu_0\left(1-{\mu_0}^2\right)F\right]}{\partial \mu_0}+\left[{\mu_0}^2\left(\frac{1}{\rho}\frac{\partial\rho}{\partial t}+\frac{3v}{r}\right)-\frac{v}{r}\right]\\&\quad\times\frac{1}{{E_0}^2}\frac{\partial\left({E_0}^3 F\right)}{\partial E_0}=\frac{1}{E_0}C[F],\end{aligned}\tag{8}$$

where $F = f/\rho$ is the specific neutrino distribution function. Note that here the Lagrangian partial derivatives with respect to t and m are at constant m and t, respectively. We can express the partial derivatives with respect to the Lagrangian spacetime coordinates, (t, m), in terms of the Eulerian spacetime coordinates, $(\tilde{t}, r)$, using

$$\frac{\partial}{\partial t} = \frac{\partial \tilde{t}}{\partial t}\frac{\partial}{\partial \tilde{t}} + \frac{\partial r}{\partial t}\frac{\partial}{\partial r}$$

and

$$\frac{\partial}{\partial m} = \frac{\partial \tilde{t}}{\partial m}\frac{\partial}{\partial \tilde{t}} + \frac{\partial r}{\partial m}\frac{\partial}{\partial r}.$$

Using Equation (45) of Cardall & Mezzacappa (2003), we have to $\mathcal{O}(v)$,

$$\frac{\partial}{\partial t} = \frac{\partial}{\partial \tilde{t}} + v\frac{\partial}{\partial r} = \frac{D}{D\tilde{t}}$$

and

$$\frac{\partial}{\partial m} = \frac{v}{4\pi r^2 \rho}\frac{\partial}{\partial \tilde{t}} + \frac{1}{4\pi r^2 \rho}\frac{\partial}{\partial r}.$$

Substituting these transformations into the first three terms in Equation (8) gives

$$\begin{aligned}\frac{\partial F}{\partial t} + 4\pi\mu_0\frac{\partial(r^2\rho F)}{\partial m} + \frac{1}{r}\frac{\partial\left[\left(1-\mu_0{}^2\right)F\right]}{\partial\mu_0} &= \frac{\partial F}{\partial \tilde{t}} + v\frac{\partial F}{\partial r} + \frac{\mu_0 v}{r^2\rho}\frac{\partial(r^2\rho F)}{\partial \tilde{t}} + \frac{\mu_0}{r^2\rho}\frac{\partial\left(r^2\rho F\right)}{\partial r} \\ &\quad + \frac{1}{r}\frac{\partial[(1-\mu_0{}^2)F]}{\partial\mu_0}. \end{aligned} \tag{9}$$

Writing the right-hand side of Equation (9) in terms of f and expanding, we are left with

$$\begin{aligned}\frac{\partial F}{\partial t} + 4\pi\mu_0\frac{\partial(r^2\rho F)}{\partial m} + \frac{1}{r}\frac{\partial\left[\left(1-\mu_0{}^2\right)F\right]}{\partial\mu_0} &= \frac{1}{\rho}\left[(1+\mu_0 v)\frac{\partial f}{\partial \tilde{t}} + (\mu_0+v)\frac{\partial f}{\partial r} + \frac{1-\mu_0{}^2}{r}\frac{\partial f}{\partial\mu_0}\right] \\ &\quad - \frac{f}{\rho^2}\frac{D\rho}{D\tilde{t}} + \mathcal{O}(v^2). \end{aligned} \tag{10}$$

Moving the term containing the Lagrangian time-derivative, $D/D\tilde{t}$, of the density to the LHS and restating it using the Lagrangian time-derivative, $\partial/\partial t$, we have to $\mathcal{O}(v)$,

$$\begin{aligned}&\frac{\partial F}{\partial t} + 4\pi\mu_0\frac{\partial(r^2\rho F)}{\partial m} + \frac{1}{r}\frac{\partial\left[\left(1-\mu_0{}^2\right)F\right]}{\partial\mu_0} + \frac{F}{\rho}\frac{\partial\rho}{\partial t} \\ &= \frac{1}{\rho}\left[(1+\mu_0 v)\frac{\partial f}{\partial \tilde{t}} + (\mu_0+v)\frac{\partial f}{\partial r} + \frac{1-\mu_0{}^2}{r}\frac{\partial f}{\partial\mu_0}\right]. \end{aligned} \tag{11}$$

Therefore, with Equation (7) as a guide, a "no-observer-correction" run in our Lagrangian formulation would correspond to a solution of the following equation:

$$\begin{aligned}&\frac{\partial F}{\partial t} + 4\pi\mu_0\frac{\partial(r^2\rho F)}{\partial m} + \frac{1}{r}\frac{\partial\left[\left(1-\mu_0{}^2\right)F\right]}{\partial\mu_0} + \frac{F}{\rho}\frac{\partial\rho}{\partial t} \\ &\qquad = \frac{1}{E_0}\frac{1}{\rho}C[f] \equiv \frac{1}{E_0}C[F]. \end{aligned} \tag{12}$$

Equation (12) is used in our "no-observer-corrections" model, N-ReducOp-NOC. Equation (12) is clearly not manifestly conservative for neutrino number when integrated over mass and when the density evolves, and therefore its Eulerian equivalent, Equation (7), is also not number conservative when integrated over volume. On the other hand, Equation (6) *is* number conservative when integrated over volume (after dropping the $\mu_0 v\partial f/\partial t$ term). The culprit in Equation (7) is the $v\partial f/\partial r$ term. When expressed in volume-conservative form, this term contains a velocity divergence, or equivalently a logarithmic time derivative of the density, that would normally be canceled by the logarithmic time derivative of the density in Equation (6). But when the observer corrections are dropped, the last term on the LHS of Equation (6) is dropped, and this cancellation no longer occurs and we are left with the same term that appears as the last term on the LHS of Equation (12), which breaks number conservation. By expressing our observer corrections in Equation (6) in conservative form, we made explicit this logarithmic time derivative of density contained within them.

3. NUMERICAL METHODS AND INPUTS

All models in this paper are computed using the parallel version of the general relativistic, spherically symmetric, neutrino radiation hydrodynamics code AGILE-BOLTZTRAN (Liebendörfer et al. 2004) with extensions that we describe here.

3.1. AGILE-BOLTZTRAN

AGILE-BOLTZTRAN is a combination of the general relativistic (GR) hydrodynamics code AGILE (Liebendörfer et al. 2002) and the neutrino transport code BOLTZTRAN (Mezzacappa & Bruenn 1993b; Mezzacappa & Messer 1999; Liebendörfer et al. 2004). AGILE solves the complete GR spacetime and hydrodynamics equations implicitly in spherical symmetry on a dynamic, moving grid. The moving grid allows adequate resolution of the shock using only $\mathcal{O}(100)$ radial zones. Recent enhancements include the use of a TVD (total variation diminishing) hydrodynamics solver (Liebendörfer et al. 2005), which improves the accuracy of advection, and the use of δm as the grid coordinate rather than the enclosed mass (Fischer et al. 2010, Section 2.1), which improves numerical accuracy when mass zones are small and density gradients are large. In Newtonian mode the gravitational mass is set equal to the baryonic mass (omitting the non-rest-mass energy contributions) and the relativistic parameters are set to their non-relativistic values: $\alpha = 1, \Gamma = 1$. BOLTZTRAN (Mezzacappa & Bruenn 1993b; Mezzacappa & Messer 1999; Liebendörfer et al. 2004) solves the GR extension of the spectral neutrino Boltzmann equation (Equation (8)) with a Gauss–Legendre (S_N) quadrature. Here we use an eight-point angular quadrature and 20 logarithmically spaced energy groups with group centers from 3 to 300 MeV. Previous studies (Mezzacappa & Bruenn 1993a; Liebendörfer et al. 2004) with (AGILE-)BOLTZTRAN have shown that 20-group energy resolution is adequate in removing artifacts seen at lower (12-group) energy resolution, and their 12- and 20-group runs exhibited no differences in outcomes. Moreover, 20-group energy resolution matches, or exceeds, the resolution used for supernova models computed with the multidimensional codes we discuss in Section 5. The discretization scheme is designed to simultaneously conserve lepton number and energy as described in Liebendörfer et al. (2004). Since we do not include any physics to distinguish between muon- and tau-flavored leptons, we use the combined species $\nu_{\mu\tau} = \{\nu_\mu, \nu_\tau\}$ and $\bar{\nu}_{\mu\tau} = \{\bar{\nu}_\mu, \bar{\nu}_\tau\}$.

For all models we use the nuclear, electron, and photon equations of state (EoS) of Lattimer & Swesty (LS EoS;

Table 1
Neutrino Opacity Summary

Interaction	FullOp Opacities	ReducOp Opacities
$\nu e^- \leftrightarrow \nu' e^-$	Schinder & Shapiro (1982)	None
$\nu e^+ \leftrightarrow \nu' e^+$		
$\nu n \leftrightarrow \nu' n$	Reddy et al. (1998)	Bruenn (1985)
$\nu p \leftrightarrow \nu' p$		
$e^- p \leftrightarrow \nu_e n$	Reddy et al. (1998)	Bruenn (1985)
$e^+ n \leftrightarrow \bar{\nu}_e p$		
$\nu A \leftrightarrow \nu A$	Bruenn (1985)	Bruenn (1985)
$\nu\alpha \leftrightarrow \nu\alpha$	Bruenn (1985)	Bruenn (1985)
$e^-(A, Z) \leftrightarrow \nu_e(A, Z-1)$	Langanke & Martínez-Pinedo (2000)	Bruenn (1985)
	Langanke et al. (2003)	
$e^- e^+ \leftrightarrow \nu\bar{\nu}$	Schinder & Shapiro (1982)	Schinder & Shapiro (1982)
$NN \leftrightarrow NN\nu\bar{\nu}$	Hannestad & Raffelt (1998)	Hannestad & Raffelt (1998)

1991) with the bulk incompressibility of nuclear matter $\kappa_s = 220$ MeV.[9] This matches the current experimental value of $\kappa_s = 240 \pm 20$ MeV (Shlomo et al. 2006) better than the value of 180 MeV more commonly used with LS EoS in the past, though the value of κ_s in LS EoS has been shown to be of little consequence during the early phases of core-collapse supernova evolution shown here (Swesty et al. 1994; Thompson et al. 2003; Lentz et al. 2010). Matter outside the "iron" core is treated as an ideal gas of ^{28}Si that "flashes" instantaneously to nuclear statistical equilibrium when the temperature exceeds 0.47 MeV.

The stellar progenitor used for all models reported here is the 15-$M_\odot$ solar-metallicity progenitor of Woosley & Heger (2007). We have mapped the inner 1.8 $M_\odot$ of the progenitor onto 108 mass shells of the adaptive radial grid.

3.2. Neutrino Opacities

The base, or full, opacity set (FullOp) includes emission, absorption, and scattering on free nucleons (Reddy et al. 1998); isoenergetic scattering on α-particles and heavy nuclei (Bruenn 1985); scattering of neutrinos on electrons (NES) and positrons (NPS; Schinder & Shapiro 1982); production of neutrino pairs from e^+e^- annihilation (Schinder & Shapiro 1982) and nucleon–nucleon bremsstrahlung (Hannestad & Raffelt 1998); and electron capture (EC) on nuclei using the LMSH EC table of Langanke et al. (2003), which utilizes the EC rates of Langanke & Martínez-Pinedo (2000). The full angle and energy exchange for scattering between the neutrinos and electrons, positrons, and nucleons is included, while scattering on nuclei is isoenergetic. Bremsstrahlung and e^-e^+ annihilation are the only sources of $\nu_{\mu\tau}$ and $\bar{\nu}_{\mu\tau}$.

For our reduced opacity set (ReducOp) we replace the LMSH EC table for electron capture on nuclei with an independent particle approximation (IPA; Fuller 1982) using the implementation described in Bruenn (1985), which cuts off when the mean neutron number of the heavy nuclei $N \geqslant 40$. We also drop all scatterings (NIS) that couple neutrino-energy groups. The primary contribution of electron and positron scattering opacities is through neutrino-energy down-scattering (Mezzacappa & Bruenn 1993c), not through their contribution to the total scattering opacity; therefore, we omit them completely from the ReducOp opacity set. We also replace the NIS nucleon scattering opacities of Reddy et al. (1998) with the more approximate IS equivalents from Bruenn (1985). For consistency, we also replace the neutrino emission and absorption opacities of Reddy et al. (1998) with their Bruenn (1985) equivalents. Ion–ion correlations and weak magnetism are omitted from both opacity sets. The two opacity sets are summarized in Table 1.

3.3. Observer Corrections

As noted in Section 2, the Lagrangian formulation in AGILE-BOLTZTRAN and the use of the specific neutrino distribution function, $F = f/\rho$, which is needed to properly account for number and energy conservation (see discussion on the necessity of using F for Lagrangian models in Cardall & Mezzacappa 2003, Section IV.B), require care in the definition of a no-observer-corrections model. Moreover, time derivatives at fixed Lagrangian mass coordinates on a moving grid must be handled with care (see Liebendörfer et al. 2004, Section 3.2). Therefore, for model N-ReducOp-NOC, we implement the "compression" term in the no-observer-corrections transport Equation (12) by re-expressing the time derivative of density as a spatial divergence, using the continuity equation,

$$\frac{F}{\rho}\frac{\partial \rho}{\partial t} = -\frac{F}{r^2}\frac{\partial (r^2 v)}{\partial r}. \tag{13}$$

4. RESULTS

We present results from four spherically symmetric, core-collapse supernova models of decreasing physical fidelity. The most physically complete model (GR-FullOp, black lines in plots) utilizes the more modern and complete FullOp opacities and the full general relativistic treatment of gravity, hydrodynamics, and transport as described in Liebendörfer et al. (2004). The first approximate model (N-FullOp, red lines) replaces the full general relativity of the GR-FullOp model with Newtonian gravity, $\mathcal{O}(v/c)$ hydrodynamics, and $\mathcal{O}(v/c)$ transport. The second approximate model (N-ReducOp, green lines) further replaces the more complete FullOp neutrino opacity set with the ReducOp opacities (see Table 1 for a full comparison), while retaining the Newtonian gravity, $\mathcal{O}(v/c)$ hydrodynamics, and $\mathcal{O}(v/c)$ transport. This approximation includes the important effect of removing neutrino weak interactions that down-scatter the neutrino energy. The final approximate model (N-ReducOp-NOC, blue lines) retains the Newtonian gravity and $\mathcal{O}(v/c)$ hydrodynamics of the previous model, but drops the observer corrections completely, reducing the transport to $\mathcal{O}(1)$. (The $\mathcal{O}(1)$ and $\mathcal{O}(v/c)$ hydrodynamics equations are identical.) The

[9] We use the latest version of the Lattimer & Swesty (1991) EoS, version 2.7, which is available for download from its authors at http://www.astro.sunysb.edu/dswesty/lseos.html.

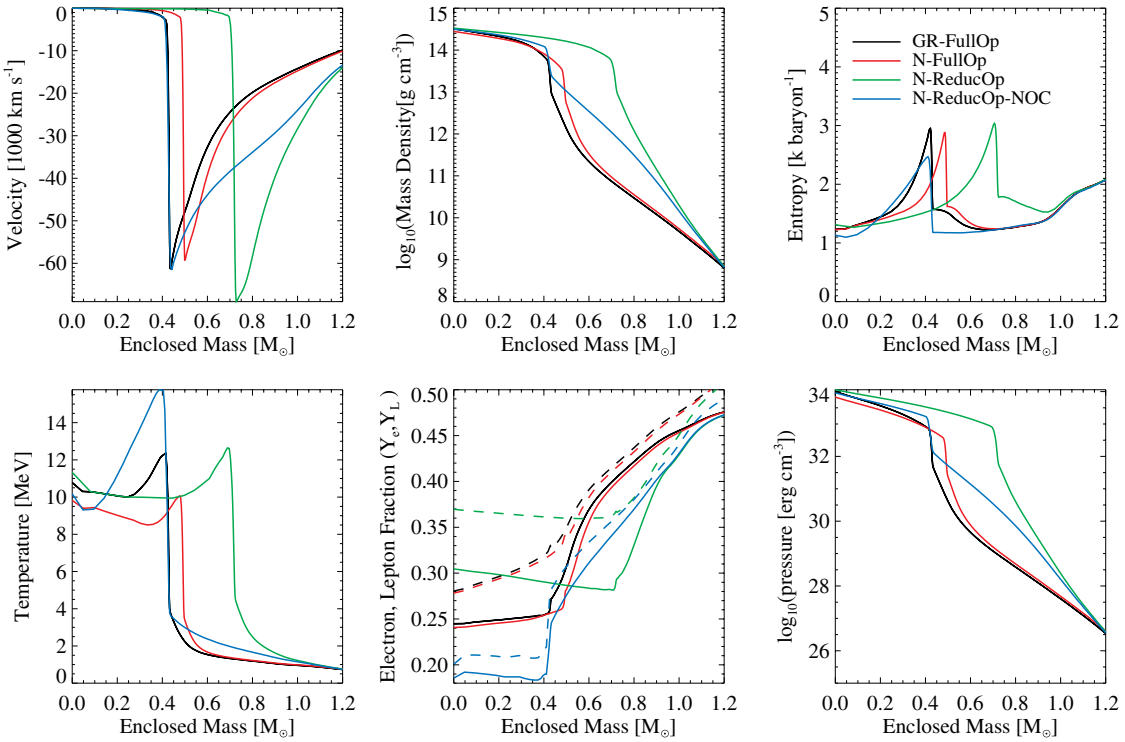

Figure 1. Properties of our models at core bounce, where bounce is defined as the maximum compression of the central density during the launch of the bounce shock. The models are: general relativistic gravity, hydrodynamics and transport with full opacities (GR-FullOp, plotted in black); Newtonian gravity with full opacities and $\mathcal{O}(v/c)$ hydrodynamics and transport (N-FullOp, plotted in red); Newtonian gravity with reduced opacities and $\mathcal{O}(v/c)$ hydrodynamics and transport (N-ReducOp, plotted in green); and Newtonian gravity with $\mathcal{O}(v/c)$ hydrodynamics and reduced opacities, and $\mathcal{O}(1)$ transport (N-ReducOp-NOC, plotted in blue). The panels are radial velocity (upper left), density (upper center), entropy (upper right), temperature (kT, lower left), net electron (or proton) fraction (Y_e, lower center, solid lines), net lepton fraction ($Y_L = Y_e + (n_{\nu_e} - n_{\bar{\nu}_e})/n_{\rm baryons}$, lower center, dashed lines), and pressure (lower right). All quantities are plotted relative to enclosed rest mass in $M_\odot$.

(A color version of this figure is available in the online journal.)

Table 2
Model Approximations and Properties

Property	GR-FullOp	N-FullOp	N-ReducOp	N-ReducOp-NOC
Gravity and hydrodynamics	GR	Newtonian	Newtonian	Newtonian
Neutrino opacities (see Table 1)	Full	Full	Reduced	Reduced
Observer corrections	GR	$\mathcal{O}(v/c)$	$\mathcal{O}(v/c)$	None
Homologous core, $M_{\rm sh}$ ($M_\odot$)	0.429	0.492	0.717	0.427
Central-core density at bounce, $\rho_{\rm c}$ ($\times 10^{14}$ g cm^{-3})	4.714	4.264	3.336	3.157
Central-core electron fraction (Y_e) at bounce	0.2448	0.2407	0.3046	0.1855
Central-core lepton fraction (Y_L) at bounce	0.2804	0.2782	0.3696	0.2007
Peak shock radius (km)	162	190	171	142
Peak ν_e-Luminosity (Bethe s^{-1})	406	450	448	160

general and core-bounce properties of all models are summarized in Table 2 and plotted in Figure 1.

4.1. GR versus Newtonian Gravity

The effects of general relativity on the core dynamics are seen in the comparison of the first two models (GR-FullOp and N-FullOp). The deeper gravitational well of the GR model results in a more compact homologous core at bounce (0.429 $M_\odot$ versus 0.492 $M_\odot$) with a higher central density (4.71×10^{14} g cm^{-3} versus 4.26×10^{14} g cm^{-3}) and higher temperatures throughout the unshocked core (Figure 1). The electron (Y_e) and lepton (Y_L) fractions are essentially unchanged modulo the shift in shock position, as are the velocity and entropy, while the pressure differences follow the density differences. As the shock moves out, the shock radius for both models (Figure 2) remains close for the first 40 ms after bounce and then diverges. The GR-FullOp model has maximum shock extent that is 30 km (20%) smaller than the N-FullOp model, and by 150 ms after bounce the shock radius is 40 km (30%) smaller. Several quantities reflect the long-term effect of the more compact, and therefore hotter, proto-NS in the GR-FullOp model, including the higher luminosities for all neutrino species (Figure 3) and the higher rms energies ($\langle E_\nu \rangle_{\rm rms}$) of neutrinos of all flavors after the breakout burst (Figure 4). These differences are in accord with those already reported by Liebendörfer et al. (2001), Bruenn et al. (2001), and Buras et al. (2006) using different progenitors, different opacity sets (similar to ReducOp, though including NES), different energy and angle resolutions, and for the latter two cases, different codes. Our GR/Newtonian comparison is included here for completeness and to facilitate relative comparisons across all four models.

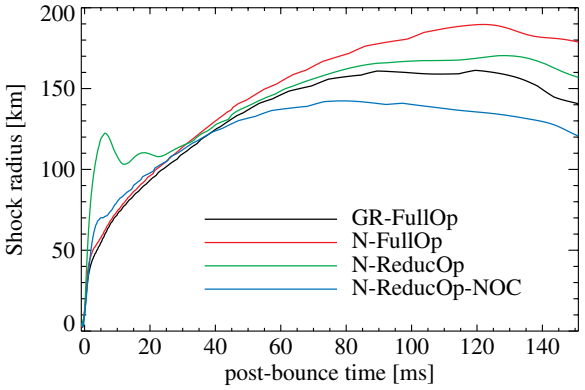

Figure 2. Shock trajectories in kilometers, vs. time after bounce, for all models. The colors have the same meaning as in Figure 1. Shock position is computed by bisecting the pair of mass shells with the largest negative radial velocity gradient $-\partial v_r/\partial r$.

(A color version of this figure is available in the online journal.)

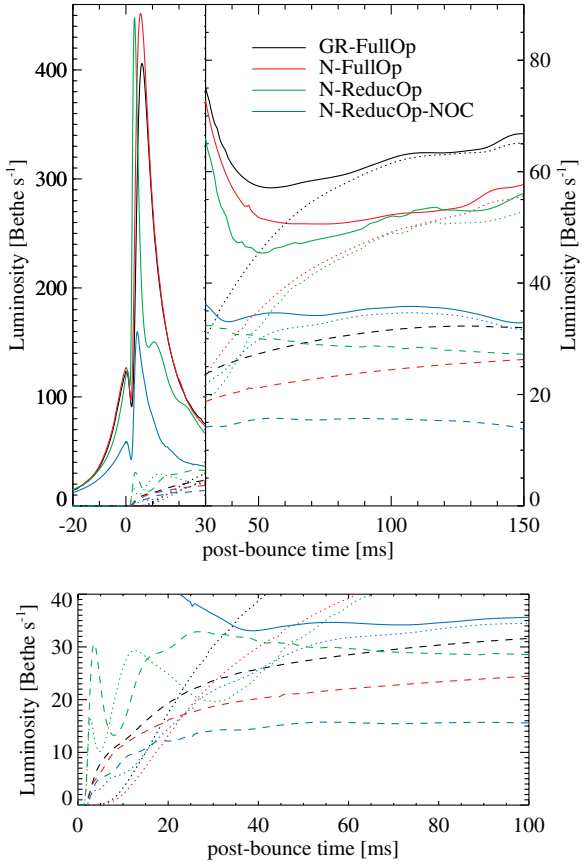

Figure 3. Comoving-frame neutrino luminosities measured at 400 km for all models. Colors are as in Figure 1. Electron neutrino, ν_e, luminosities are represented by solid lines, $\bar{\nu}_e$-luminosities by dotted lines, and $\nu_{\mu\tau}$-luminosities by dashed lines. $\bar{\nu}_{\mu\tau}$-luminosities are indistinguishable from $\nu_{\mu\tau}$-luminosities, and are omitted from this figure. The luminosities are in Bethe s^{-1}, where 1 Bethe = 10^{51} ergs. The lower panel provides a detailed view of the luminosities below 40 Bethe s^{-1} during the first 100 ms after bounce.

(A color version of this figure is available in the online journal.)

4.2. Reduced Neutrino Opacities

The changes induced as we go from the FullOp opacities (model N-FullOp) to the ReducOp opacities (model N-ReducOp) in the Newtonian-gravity, $\mathcal{O}(v/c)$-hydrodynamics,

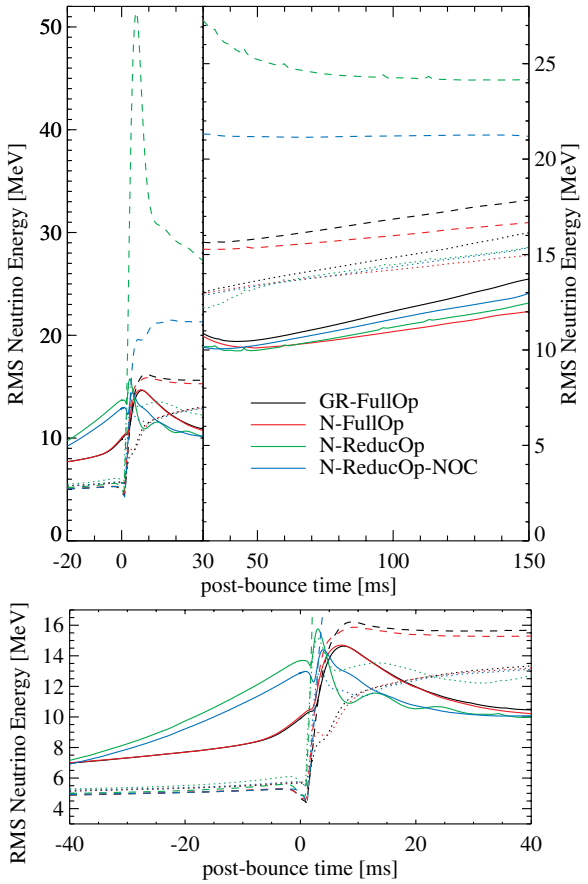

Figure 4. Comoving-frame neutrino rms energies, $\langle E_\nu\rangle_{\rm rms} = (\int d\mu\, dE\, E^4 F/\int d\mu\, dE\, E^2 F)^{1/2}$, measured at 400 km for all models. rms energy is computed over number density, not number flux. Colors are as in Figure 1. Line styles are as in Figure 3. The lower panel provides a detailed view of $\langle E_\nu\rangle_{\rm rms}$ for values less than 20 MeV over the period ±40 ms.

(A color version of this figure is available in the online journal.)

and $\mathcal{O}(v/c)$-transport limit are more dramatic than those seen for the transition from models GR-FullOp to N-FullOp in Section 4.1. The shock position at bounce changes from 0.492 $M_\odot$ for N-FullOp to 0.717 $M_\odot$ for N-ReducOp (Figure 1), with the entropy peak (upper right) making the same shift. The increase in the initial shock mass, $M_{\rm sh}$, is correlated with the corresponding increase in core lepton fraction, from $Y_L = 0.28$ to 0.37 ($M_{\rm sh} \propto Y_L^2$). The larger $M_{\rm sh}$ for N-ReducOp, relative to the other models, results in a correspondingly larger region of high pressure, temperature, and density at bounce. The vigorous post-bounce shock of model N-ReducOp results in a strong "ringing" of the shock (Figure 2). Thompson et al. (2003) reported a similar ringing for their "no NES" model.

The ν_e-luminosity of the N-ReducOp model reaches the same peak value as in the N-FullOp model, 450 Bethe s^{-1}, but the breakout burst is much shorter in duration and represents a smaller total emission of ν_e. The shock starts out at a larger mass coordinate and passes through less total mass before becoming a steady accretion shock. Like Thompson et al. (2003), we see oscillations of the ν-luminosities and $\langle E_\nu\rangle_{\rm rms}$ (Figures 3 and 4) just after bounce induced by shock oscillations passing through the neutrinospheres.

The differences between the N-FullOp and N-ReducOp models can be understood by considering three opacity changes *imposed simultaneously*: (1) the inclusion of NES/NPS; (2) the

use of the LMSH EC table; and (3) the use of the Reddy et al. (1998) nucleon opacities.

1. The effects of omitting the NES opacity *alone* during collapse were explored by Mezzacappa & Bruenn (1993c), who showed that energy down-scattering by NES allowed the energy down-scattered neutrinos to escape more easily because of the lower absorption and scattering cross sections at lower energies, and reduced the core Y_e by 15% and neutrino fraction, Y_ν, by 30% in their model with NES relative to one without NES. The higher number of trapped neutrinos, without NES, is reflected in the higher core Y_e, Y_L, and Y_ν for our model N-ReducOp. The "no-NES" model of Thompson et al. (2003, Section 7.4, Figures 20 and 21) also shows large differences in $\langle E_{\nu_{\mu\tau}}\rangle_{\rm rms}$, with a bounce "spike" reaching 32 MeV, and a $\langle E_{\nu_{\mu\tau}}\rangle_{\rm rms}$ increase at 150 ms post-bounce of 4 MeV (20%) relative to a model with NES. This compares to a 50 MeV "spike" and 7 MeV (40%) increase at 150 ms after bounce in $\langle E_{\nu_{\mu\tau}}\rangle_{\rm rms}$ for our N-ReducOp model relative to our N-FullOp model.
2. We have removed the LMSH EC table from ReducOp opacities in favor of the simpler IPA prescription, as not all modern supernova simulations use EC rates like the LMSH EC table, which reflect the ensemble of nuclei and their excited states in the collapsing core. Hix et al. (2003) found that the enhanced EC arising from the removal of the artificial cutoff in IPA for heavier nuclei that occur at higher densities during collapse decreased the central-core Y_e and $M_{\rm sh}$ at bounce by 10% and 20%, respectively, relative to the IPA implementation. Conversely, IPA overestimates EC where it is active and leads to excess deleptonization and stronger collapse in the outer regions of the Fe-core where the $N \geqslant 40$ cutoff criterion is not triggered. One such region can be seen at bounce outside the homologous core near $0.9\,M_\odot$ (Figure 1), where lower Y_e and higher density exist in the N-ReducOp model relative to the GR-FullOp and N-FullOp models.
3. We have also replaced the ν-nucleon emission, absorption, and scattering opacities (Reddy et al. 1998) in FullOp with the corresponding opacities of Bruenn (1985) to eliminate neutrino-energy down-scattering on nucleons. We have previously found (Lentz et al. 2010) that the inclusion of the enhanced nucleon opacities results in an enhancement of the luminosities, but not rms energies, and lifts the post-bounce shock outward by 10 km by 100 ms post-bounce through absorption of the excess luminosity. These findings are consistent with the results of Rampp et al. (2002) on the enhanced neutrino–nucleon opacities.

4.3. No Observer Corrections

For the final comparison we change the treatment of the observer corrections in the transport equation. In model N-ReducOp-NOC we have removed the velocity-dependent observer corrections from the Boltzmann transport equation in the appropriate, Lagrangian approach as described by Section 2, Equation (12), but retain the Newtonian gravity, $\mathcal{O}(v/c)$-hydrodynamics, and reduced opacities of the N-ReducOp model.

Dropping the observer corrections in model N-ReducOp-NOC results in a dramatic change in the properties of the core at bounce, as can be seen in Figure 1 and Table 2. The homologous core mass drops from $0.717\,M_\odot$ for the N-ReducOp model to $0.427\,M_\odot$ for the N-ReducOp-NOC model; the latter of which is virtually indistinguishable from the homologous core mass, $M_{\rm sh}$, for the most physically complete model ($0.429\,M_\odot$ for GR-FullOp). This coincidental alignment of the bounce shock positions for the most and least physically complete models should be contrasted with the lower electron and lepton fractions (Y_e, Y_L) and density (see Table 2) in the homologous core for the N-ReducOp-NOC model relative to the GR-FullOp model, as well as the larger inflow velocities and densities and lower Y_e and Y_L outside the shock, which imply, among other things, an increased ram pressure against which the shock must propagate.

The shock (Figure 2) in the N-ReducOp-NOC model starts more vigorously than in the FullOp models, but does not show the large overshoot of the other reduced opacity model, N-ReducOp. All of the shock trajectories cross near 35 ms after bounce, with the N-ReducOp-NOC model having the deepest shock throughout the rest of the run. This is in stark contrast to the other Newtonian models, which have larger shock radii relative to the GR-FullOp model.

The neutrino luminosities (Figure 3) of the N-ReducOp-NOC model are also substantially lower than for any other model. The ν_e-luminosity from shock-breakout peaks at 160 Bethe $\rm s^{-1}$ for the N-ReducOp-NOC model relative to the 400–450 Bethe $\rm s^{-1}$ for the models with observer corrections. The $\bar{\nu}_e$-luminosities of all models approaches the ν_e-luminosities at around 80 ms after bounce, and track together thereafter. By 150 ms after bounce, the $\nu_e\bar{\nu}_e$-luminosities for the N-ReducOp-NOC model are approximately 32 Bethe $\rm s^{-1}$, while the other two Newtonian models have $\nu_e\bar{\nu}_e$-luminosities of approximately 55 Bethe $\rm s^{-1}$ and the GR-FullOp model has $\nu_e\bar{\nu}_e$-luminosities of approximately 66 Bethe $\rm s^{-1}$.

The rms neutrino energies (Figure 4) for ν_e (solid lines) and $\bar{\nu}_e$ (dotted lines) in the N-ReducOp-NOC model follow those in the N-ReducOp model closely, with $\langle E_{\nu_e}\rangle_{\rm rms}$ slightly higher before bounce and at later times, except in the immediate post-bounce period when it oscillates in the N-ReducOp model with the shock. In contrast, the post-bounce $\langle E_{\nu_{\mu\tau}}\rangle_{\rm rms}$ for model N-ReducOp-NOC is substantially lower relative to model N-ReducOp, and the "spike" after bounce is gone. After breakout both ReducOp models have large $\langle E_{\nu_{\mu\tau}}\rangle_{\rm rms}$ relative to the FullOp-models.

As we traverse our four models, it is clear that all of the neutrino luminosities are significantly affected. The general trend is for the luminosities to decrease considerably as we go from GR-FullOp to N-FullOp to N-ReducOp to N-ReducOp-NOC. The largest variations among the models are exhibited by the electron-flavor neutrinos, with luminosity variations as large as 35 Bethe $\rm s^{-1}$ at 150 ms after bounce. However, the variations in the $\langle E_{\nu_e}\rangle_{\rm rms}$ and $\langle E_{\bar{\nu}_e}\rangle_{\rm rms}$ are not as dramatic as we traverse the four models, and not monotonically decreasing as the model sophistication decreases. Variations in the $\langle E_{\nu_{\mu\tau}}\rangle_{\rm rms}$, like their luminosity counterparts, remain significant, although not monotonically decreasing with model. The post-bounce rms energies, $\langle E_{\nu_{\mu\tau}}\rangle_{\rm rms}$, vary by $\sim$10 MeV up to 150 ms after bounce.

At 100 ms after bounce (Figure 5) the shock encloses $1.45\,M_\odot$ for all four models. The most significant differences seen in the dense core are in Y_e and Y_L (lower center), where the N-ReducOp-NOC model has generally the lowest Y_e and Y_L and lacks the peak the other models exhibit just outside their bounce shock positions, $M_{\rm sh}$. Figure 6 shows the same data, but focuses on the outer, "hot-mantle" region between the shock and proto-NS with the most evident differences being those related to the shock radius (smallest for N-ReducOp-NOC). Though shifted in radius, the hot-mantle region is similar among all models.

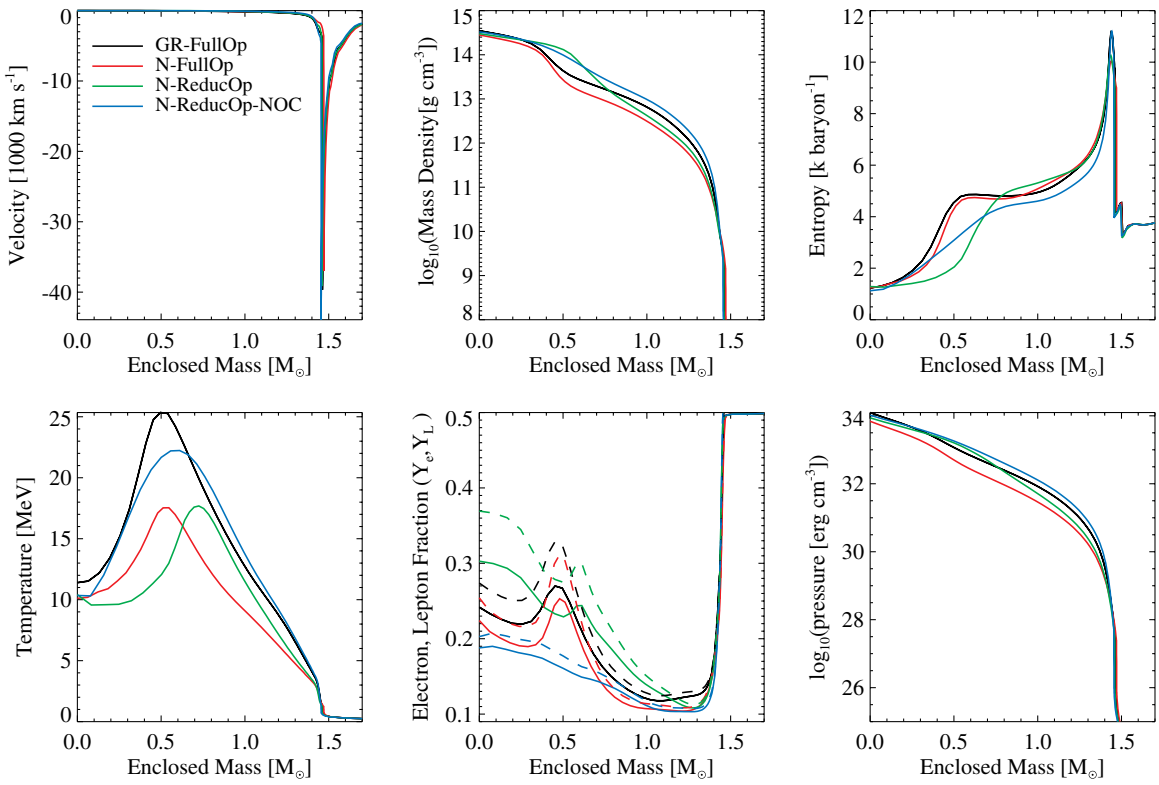

Figure 5. Same as in Figure 1, but at 100 ms after core bounce.
(A color version of this figure is available in the online journal.)

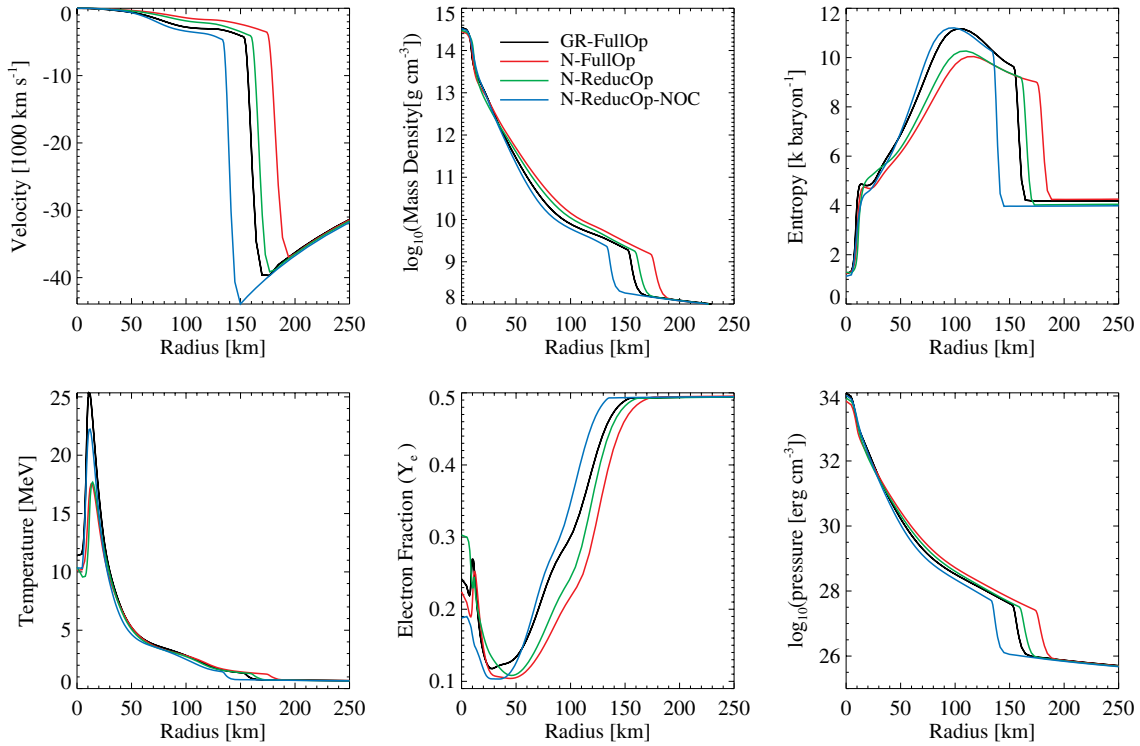

Figure 6. Same as in Figure 5, but as a function of radial coordinate, r, in kilometers. Net lepton number has been omitted, as $Y_L \approx Y_e$ for all but the inner few kilometers.
(A color version of this figure is available in the online journal.)

The N-ReducOp-NOC model shows (Figure 7) a drop in total conserved lepton number ($N_{\mathrm{L,cons}}$, the lepton number on the computational grid plus the time-integrated number flux of neutrinos at the outer boundary) starting just before bounce and continuing throughout the rest of the run. This is not seen in the other models, which maintain lepton conservation. The root of the non-conservation can be seen in the integration of Equation (12) for neutrino number over the entire grid.

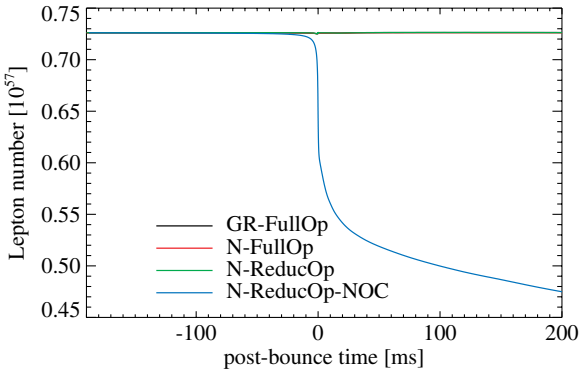

Figure 7. Lepton number on the grid plus neutrino flux through the outer boundary, $N_{\rm L,cons}$, indicating the quality of numerical lepton conservation for all models. Model N-ReducOp-NOC loses 34.7% of the original $N_{\rm L,cons}$ by 200 ms after bounce, while the other three models conserve $N_{\rm L,cons}$ to within 0.1%.

(A color version of this figure is available in the online journal.)

It results from the $(F/\rho)(\partial\rho/\partial t)$ "compression" term and is strongest during the epoch of high Y_ν and rapid density changes surrounding core bounce.

We illustrate this loss through Y_e (Figure 8, solid lines) and Y_L (dashed lines) profiles for the GR-FullOp model (upper panel) and the N-ReducOp-NOC model (lower panel) as a series of temporal snapshots near bounce. Until the shock reaches 0.5 $M_\odot$ in the GR-FullOp model (upper panel), the core is still opaque, and the neutrinos are trapped. Therefore, total lepton number is conserved locally, and Y_L is steady inside 0.5 $M_\odot$ during shock breakout as depicted in the upper panel of Figure 8. When the shock reaches 0.5 $M_\odot$, it begins to break through the neutrinospheres, and the neutrinos can escape, causing the local Y_L and Y_e to drop behind the shock. The escaping neutrinos contribute to Y_L in front of the shock as a visible pulse, a small portion of which are absorbed by the cold, infalling matter ahead of the shock, forming a transient radiative precursor in Y_e. For the N-ReducOp-NOC model (lower panel) there is no such corresponding epoch of local lepton conservation as the shock forms in the opaque (neutrino trapped) inner core before emerging through the neutrinospheres. The net effect of the compression term in Equation (12) is one of destroying neutrinos, which then results in a net decrease in Y_e via the interactions $e^- p \leftrightarrow \nu_e n$ and $e^+ n \leftrightarrow \bar{\nu}_e p$. The loss of neutrinos to the compression term reduces the neutrino pulse ahead of the shock and lowers the ν_e-luminosity in the breakout burst (Figure 3).

The fundamentally different behavior of the N-ReducOp-NOC model stems from two factors: (1) the omission of the energy derivative term in Equation (8) or the equivalent term in Equation (6); and (2) the fact that Equation (12) is manifestly non-conservative for neutrino, and consequently lepton, number when integrated over mass. In the neutrino opaque regions, the energy-derivative term is responsible for promoting neutrinos in energy as they are compressed, as expected for a relativistic Fermi gas and first noted by Castor (1972) and Arnett (1977).

5. CONTEMPORARY MULTIDIMENSIONAL SUPERNOVA MODELING

5.1. Multidimensional Supernova Codes

There are five extant codes that can compute the spectral neutrino radiation hydrodynamics for core-collapse supernova simulations in 2D or 3D. These codes are (in alphabetical order):

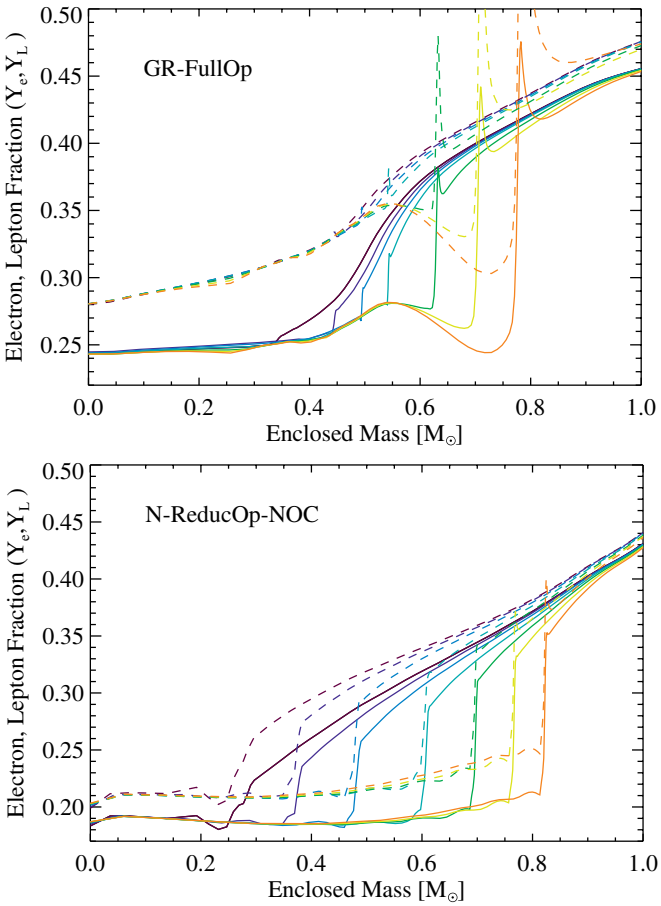

Figure 8. Sequence of electron (solid lines) and lepton (dashed lines) fraction profiles for the GR-FullOp (upper panel) and N-ReducOp-NOC (lower panel) models showing the formation of the shock and the shock progress through bounce into the breakout phase. The colors represent different epochs, which are equally spaced in computational time step with time advancing from dark to light gray (violet to red in the online journal).

(A color version of this figure is available in the online journal.)

the 2D/3D code CHIMERA (S. W. Bruenn et al. 2012, in preparation), the 2D code V2D (Swesty & Myra 2009, 2005), the 2D code Vertex (Rampp & Janka 2002; Buras et al. 2006), the 2D code Vulcan/2D (Livne et al. 2004; Burrows et al. 2007), and the 2D/3D Zeus+IDSA code (Suwa et al. 2010).

Of the multidimensional codes, CHIMERA and (Prometheus-)Vertex include a spherically symmetric, post-Newtonian GR approximation, while the others are strictly Newtonian in their gravitation, hydrodynamics, and neutrino transport. Müller et al. (2010) have updated (CoCoNuT-) Vertex to include general relativity in the transport and hydrodynamics using the conformally flat approximation.

CHIMERA, V2D, and Vulcan/2D transport neutrinos by the flux-limited diffusion method (FLD). Vulcan/2D also has a non-moment, multi-angle (S_N) mode. Vertex uses the variable Eddington tensor (VET) method with a closure computed using a spherically averaged, model Boltzmann equation. The Zeus+IDSA code uses the Isotropic Diffusion Source Approximation (IDSA; Liebendörfer et al. 2009), which divides the neutrinos into "trapped' and "free-streaming" neutrinos, with a diffusion source to connect them.

Of these codes, only V2D is capable of solving the full space-neutrino energy–species coupling of the neutrino transport that the core-collapse supernova problem requires, while all other codes break at least one aspect of that coupling to

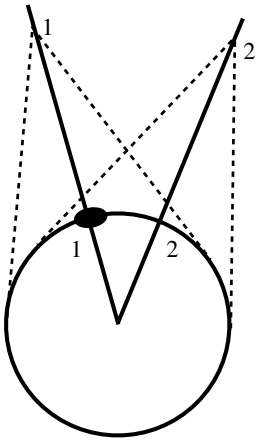

Figure 9. Illustration of the "ray-by-ray" transport approximation. The circle represents the neutrinosphere and the solid lines represent two independent "rays" in the RbR approximation. The dashed lines are tangents to the neutrinosphere and indicate the regions that contribute to the neutrino field at points 1 and 2. The "blob" on the neutrinosphere below point 1 is a "hot spot" where the temperature is higher than the rest of the neutrinosphere. For point 1, the RbR method will compute the neutrino field as if the entire neutrinosphere has the properties of the hot spot, overestimating the neutrino flux and heating. For point 2, the RbR misses the contribution of the hot spot by assuming that the neutrinosphere properties are only those of the cooler region directly below it, underestimating the neutrino flux and heating.

reduce computational costs and simplify code development. CHIMERA, Vertex, and Zeus+IDSA break the non-radial (lateral, or angular) spatial coupling through the "ray-by-ray" (RbR) approximation, and Vulcan/2D breaks the coupling between energy groups and neutrino species.

In the RbR approximation, the neutrino transport is computed as a number of independent, spherically symmetric problems, referred to as "rays," which allows for the reuse of existing 1D neutrino transport codes. (See Figure 9 for a schematic illustration of the RbR approximation.) RbR methods exhibit good parallel scaling for large numbers of independent radial rays, which can be evolved without communication while computing the neutrino transport. Typically, in RbR codes, the neutrinos in opaque regions are advected laterally with the fluid motions and contribute to the pressure. The independence of the rays artificially sharpens the lateral variation in the neutrino luminosity and heating above the proto-NS, which results in some regions of the hot mantle being overheated and others underheated. The transport studies of Ott et al. (2008) using Vulcan/2D in multi-angle mode showed that full multidimensional FLD underestimates the lateral variation in the neutrino radiation field, whereas RbR codes are expected to overestimate the lateral variation. Buras et al. (2006) concluded from analysis of their RbR models that the transient lateral variations in neutrino flux and heating were not very likely to have dynamical consequences for the evolution of their models. The impact of the RbR approximation on the simulation outcomes is not precisely known, and proper testing will have to wait until one of the RbR codes is upgraded to include full lateral transport, as no extant code is currently capable of computing in RbR and non-RbR modes and there are significant differences between extant RbR and non-RbR codes in other respects.

The authors of Vulcan/2D have chosen to break the energy and species coupling rather than the lateral spatial coupling. Vulcan/2D implements computational parallelism by solving for 2D-spatially-coupled neutrino transport for each energy–species group independently, with communication only after transport to integrate neutrino heating/cooling from all energy groups. The consequence of this design choice is that Vulcan/2D cannot easily include either NIS-driven coupling of energy groups or the coupling of energy groups through observer corrections, nor can it utilize more parallel processing elements than it has energy–species groups.

5.2. Opacity Approximations

CHIMERA and Vertex include all of the FullOp opacities plus additional corrections for weak magnetism and ion–ion correlations. Vertex also includes the neutrino-pair flavor-conversion process (Buras et al. 2003). V2D uses the Bruenn (1985) opacities, which are similar to ReducOp, but do include the energy down-scattering from NES. Vulcan/2D omits all of the NIS scatterings in favor of their IS counterparts, as does the Zeus+IDSA code because energy-coupled scattering has not yet been developed for the IDSA transport method. Vulcan/2D, V2D, and Zeus+IDSA use an IPA for EC on nuclei, which cuts off electron capture by nuclei when the mean neutron number $N \geqslant 40$, and overestimates it above the cutoff, while CHIMERA and Vertex use the more accurate LMSH EC table.

Some multidimensional supernova codes (Vertex, Vulcan/2D) use a single species, $\nu_x = \{\nu_{\mu\tau}, \bar{\nu}_{\mu\tau}\}$, to represent all of the heavy-lepton flavor neutrinos, while the Zeus+IDSA code omits them completely.

5.3. Observer Corrections

CHIMERA, V2D, and Vertex include the observer corrections in the neutrino transport. In the Zeus+IDSA code, adiabatic compression is properly handled for the trapped neutrinos, and $\mathcal{O}(v/c)$ observer corrections are included for free-streaming neutrinos. These codes use neutrino transport based on Equation (3), its equivalent to $\mathcal{O}(v/c)$, or its GR equivalent. Only Vulcan/2D neglects the observer corrections entirely, by solving the neutrino transport based on Equation (7). (The transport equation quoted in Livne et al. (2004) also omits the $\mu_0 v\, \partial f/\partial t$-term, which is typically considered of $\mathcal{O}(v^2/c^2)$ and dropped from most $\mathcal{O}(v/c)$ transport solutions.)

6. CONCLUSIONS

We have examined the consequences of removing (1) GR effects, (2) non-isoenergetic scattering and detailed nuclear EC opacities, and (3) observer corrections from spherically symmetric models of core-collapse supernovae. We have found that all of these changes, individually and especially when taken together, affect the progress of stellar collapse and the post-bounce evolution of the shock and core thermodynamic properties in significant ways, in contrast to the assessments made by Burrows et al. (2006, 2007) and Nordhaus et al. (2010). We have computed variations in the shock radius, neutrino luminosities, and neutrino rms energies as large as 60 km, 35 Bethe s^{-1}, and 10 MeV, respectively, across the four models considered here.

Omission of GR results in a less compact core and an unrealistically more favorable shock progression after bounce. Eliminating non-isoenergetic scatterings and simplifying electron capture on nuclei drastically reduces the core deleptonization and expands the homologous core at bounce. Omission of the observer corrections dramatically alters core deleptonization, the shock position, and neutrino luminosities after bounce, in part resulting from a complete breakdown of lepton number conservation.

The lepton non-conservation and non-promotion of neutrino energy resulting from omitting observer corrections in our N-ReducOp-NOC model results in a compact, low-Y_L core and a shock trajectory that is the least favorable of our models. The artificial loss of lepton number, lower neutrino luminosities, and the consequent lower neutrino heating rate and shallower shock trajectory may explain the lack of neutrino-driven explosions in models computed with Vulcan/2D (see Burrows et al. 2007), in contrast to the results reported by others (Marek & Janka 2009; Bruenn et al. 2009; Suwa et al. 2010; Takiwaki et al. 2011).

Moreover, the changes in Y_e and Y_L, their gradients, and the entropy gradients that we see as we traverse the models shown here will change the location and strength of convectively unstable regions in the proto-NS and between the proto-NS and the shock. The lepton and entropy gradients in the proto-NS drive prompt convection, the entropy gradients between the proto-NS and the shock drive neutrino-driven convection, and these in turn seed and are seeded by the SASI. That is, the changes we have documented in this transport study have implications for all of the multidimensional phenomena we know to be important in multidimensional supernova models once spherical symmetry is broken.

All of the ingredients (1)–(3) above must be included in multidimensional simulations of core-collapse supernovae to ensure physical fidelity. Their omission is not the only approximation used in current multidimensional simulations, some of which (like the ray-by-ray approximation) are inadequately understood and need to be better understood or phased out. Certainly, further examination of these approximations is required within the context of multidimensional simulations.

E.J.L. is supported by grants from the NASA Astrophysics Theory and Fundamental Physics Program (grant No. NNH11AQ72I) and the NSF PetaApps Program (grant No. OCI-0749242). A.M. and W.R.H. are supported by the Department of Energy Office of Nuclear Physics; and A.M. and O.E.B.M. are supported by the Department of Energy Office of Advanced Scientific Computing Research. M.L. is supported by the Swiss National Science Foundation (grant Nos. PP00P2-124879 and 200020-122287). This research was supported in part by the National Science Foundation through TeraGrid resources provided by National Institute for Computational Sciences under grant number TG-MCA08X010. This research used resources of the Oak Ridge Leadership Computing Facility at the Oak Ridge National Laboratory, which is supported by the Office of Science of the U.S. Department of Energy under Contract No. DE-AC05-00OR22725.

REFERENCES

Arnett, W. D. 1977, ApJ, 218, 815
Bethe, H. A., & Wilson, J. R. 1985, ApJ, 295, 14
Bionta, R. M., Blewitt, G., Bratton, C. B., Casper, D., & Ciocio, A. 1987, Phys. Rev. Lett., 58, 1494
Bruenn, S. W. 1985, ApJS, 58, 771
Bruenn, S. W., De Nisco, K. R., & Mezzacappa, A. 2001, ApJ, 560, 326
Bruenn, S. W., Mezzacappa, A., Hix, W. R., et al. 2009, J. Phys.: Conf. Ser., 180, 012018
Buras, R., Janka, H., Keil, M. T., Raffelt, G. G., & Rampp, M. 2003, ApJ, 587, 320
Buras, R., Rampp, M., Janka, H.-T., & Kifonidis, K. 2006, A&A, 447, 1049
Burrows, A., Livne, E., Dessart, L., Ott, C. D., & Murphy, J. 2006, ApJ, 640, 878
Burrows, A., Livne, E., Dessart, L., Ott, C. D., & Murphy, J. 2007, ApJ, 655, 416
Cardall, C. Y., Lentz, E. J., & Mezzacappa, A. 2005, Phys. Rev. D, 72, 043007
Cardall, C. Y., & Mezzacappa, A. 2003, Phys. Rev. D, 68, 023006
Castor, J. I. 1972, ApJ, 178, 779
Colgate, S. A., & White, R. H. 1966, ApJ, 143, 626
Fischer, T., Whitehouse, S. C., Mezzacappa, A., Thielemann, F.-K., & Liebendörfer, M. 2010, A&A, 517, A80
Fuller, G. M. 1982, ApJ, 252, 741
Hannestad, S., & Raffelt, G. 1998, ApJ, 507, 339
Hirata, K., Kajita, T., Koshiba, M., Nakahata, M., & Oyama, Y. 1987, Phys. Rev. Lett., 58, 1490
Hix, W. R., Messer, O. E. B., Mezzacappa, A., et al. 2003, Phys. Rev. Lett., 91, 201102
Hubeny, I., & Burrows, A. 2007, ApJ, 659, 1458
Langanke, K., & Martínez-Pinedo, G. 2000, Nucl. Phys. A, 673, 481
Langanke, K., Martínez-Pinedo, G., Sampaio, J. M., et al. 2003, Phys. Rev. Lett., 90, 241102
Lattimer, J., & Swesty, F. D. 1991, Nucl. Phys. A, 535, 331
Lentz, E. J., Hix, W. R., Baird, M. L., Messer, O. E. B., & Mezzacappa, A. 2010, in Proc. 11th Symp. on Nuclei in the Cosmos, PoS(NIC XI)152
Liebendörfer, M., Messer, O. E. B., Mezzacappa, A., et al. 2004, ApJS, 150, 263
Liebendörfer, M., Mezzacappa, A., Thielemann, F.-K., et al. 2001, Phys. Rev. D, 63, 103004
Liebendörfer, M., Rampp, M., Janka, H.-T., & Mezzacappa, A. 2005, ApJ, 620, 840
Liebendörfer, M., Rosswog, S., & Thielemann, F.-K. 2002, ApJS, 141, 229
Liebendörfer, M., Whitehouse, S. C., & Fischer, T. 2009, ApJ, 698, 1174
Livne, E., Burrows, A., Walder, R., Lichtenstadt, I., & Thompson, T. A. 2004, ApJ, 609, 277
Marek, A., & Janka, H.-T. 2009, ApJ, 694, 664
Mezzacappa, A., & Bruenn, S. W. 1993a, ApJ, 405, 637
Mezzacappa, A., & Bruenn, S. W. 1993b, ApJ, 405, 669
Mezzacappa, A., & Bruenn, S. W. 1993c, ApJ, 410, 740
Mezzacappa, A., & Matzner, R. A. 1989, ApJ, 343, 853
Mezzacappa, A., & Messer, O. E. B. 1999, J. Comput. Appl. Math., 109, 281
Mihalas, D., & Klein, R. I. 1982, J. Comput. Phys., 46, 97
Müller, B., Janka, H.-T., & Dimmelmeier, H. 2010, ApJS, 189, 104
Nordhaus, J., Burrows, A., Almgren, A., & Bell, J. 2010, ApJ, 720, 694
Ott, C. D., Burrows, A., Dessart, L., & Livne, E. 2008, ApJ, 685, 1069
Rampp, M., Buras, R., Janka, H., & Raffelt, G. 2002, in Proc. 11th Workshop on Nuclear Astrophysics, ed. W. Hillebrandt & E. Müller (Germany: MPA), 119
Rampp, M., & Janka, H.-T. 2002, A&A, 396, 361
Reddy, S., Prakash, M., & Lattimer, J. M. 1998, Phys. Rev. D, 58, 013009
Schinder, P. J., & Shapiro, S. L. 1982, ApJS, 50, 23
Shlomo, S., Kolomietz, V. M., & Colò, G. 2006, Eur. Phys. J. A, 30, 23
Sumiyoshi, K., Yamada, S., Suzuki, H., et al. 2005, ApJ, 629, 922
Suwa, Y., Takiwaki, T., Whitehouse, S. C., Liebendörfer, M., & Sato, K. 2010, PASP, 62, L49
Swesty, F. D., Lattimer, J. M., & Myra, E. S. 1994, ApJ, 425, 195
Swesty, F. D., & Myra, E. S. 2005, J. Phys.: Conf. Ser., 16, 380
Swesty, F. D., & Myra, E. S. 2009, ApJS, 181, 1
Takiwaki, T., Kotake, K., & Suwa, Y. 2011, ApJ, in press (arXiv:1108.3989)
Thompson, T. A., Burrows, A., & Pinto, P. A. 2003, ApJ, 592, 434
Wilson, J. R. 1985, in Numerical Astrophysics, ed. J. M. Centrella, J. M. LeBlanc, & R. L. Bowers (Boston: Jones and Bartlett), 422
Woosley, S. E., & Heger, A. 2007, Phys. Rep., 442, 269